# MAVEN IUVS observations of the aftermath of the Comet Siding Spring meteor shower on Mars

N. M. Schneider, Justin I. Deighan, A. I. F. Stewart, W. E. Mcclintock, S. K. Jain, M. S. Chaffin, Arnaud Stiepen, M. Crismani, J. M. C. Plane, J. D. Carrillo-Sánchez, et al.

AGU PUBLICATIONS

Geophysical Research Letters

RESEARCH LETTER
10.1002/2015GL063863

Special Section:
Effects of the Comet C/2013 A1 (Siding Spring) meteor shower in 2014 on Mars atmosphere and ionosphere: Observations from MAVEN, Mars Express, and Mars Reconnaissance Orbiter

# MAVEN IUVS observations of the aftermath of the Comet Siding Spring meteor shower on Mars

**N. M. Schneider[1], J. I. Deighan[1], A. I. F. Stewart[1], W. E. McClintock[1], S. K. Jain[1], M. S. Chaffin[1], A. Stiepen[1], M. Crismani[1], J. M. C. Plane[2], J. D. Carrillo-Sánchez[2], J. S. Evans[3], M. H. Stevens[4], R. V. Yelle[5], J. T. Clarke[6], G. M. Holsclaw[1], F. Montmessin[7], and B. M. Jakosky[1]**

[1]Laboratory for Atmospheric and Space Physics, University of Colorado at Boulder, Boulder, Colorado, USA, [2]School of Chemistry, University of Leeds, Leeds, UK, [3]Computational Physics, Inc., Springfield, Virginia, USA, [4]Space Science Division, Naval Research Laboratory, Washington, District of Columbia, USA, [5]Lunar and Planetary Laboratory, University of Arizona, Tucson, Arizona, USA, [6]Center for Space Physics, Boston University, Boston, Massachusetts, USA, [7]LATMOS/IPSL, Guyancourt, France

**Abstract** We report the detection of intense emission from magnesium and iron in Mars' atmosphere caused by a meteor shower following Comet Siding Spring's close encounter with Mars. The observations were made with the Imaging Ultraviolet Spectrograph, a remote sensing instrument on the Mars Atmosphere and Volatile EvolutioN spacecraft orbiting Mars. Ionized magnesium caused the brightest emission from the planet's atmosphere for many hours, resulting from resonant scattering of solar ultraviolet light. Modeling suggests a substantial fluence of low-density dust particles 1–100 μm in size, with the large amount and small size contrary to predictions. The event created a temporary planet-wide ionospheric layer below Mars' main dayside ionosphere. The dramatic meteor shower response at Mars is starkly different from the case at Earth, where a steady state metal layer is always observable but perturbations caused by even the strongest meteor showers are challenging to detect.

**Key Points:**
- MAVEN/IUVS observed bright emission from vaporized dust in Mars' atmosphere
- The dust originated in an intense meteor shower caused by Comet Siding Spring
- Mars appears to respond to meteor ablation very differently than Earth does

**Correspondence to:**
N. M. Schneider,
nick.schneider@lasp.colorado.edu

**Citation:**
Schneider, N. M., et al. (2015), MAVEN IUVS observations of the aftermath of the Comet Siding Spring meteor shower on Mars, *Geophys. Res. Lett.*, *42*, 4755–4761, doi:10.1002/2015GL063863.

Received 15 MAR 2015
Accepted 15 MAY 2015
Published online 16 JUN 2015



## 1. Introduction

Shortly after the discovery of Comet Siding Spring (C/2013 A1), orbit determinations identified a very close passage by Mars on 19 October 2014. Motivated by concerns over spacecraft safety, detailed modeling of cometary dust predicted relatively low risk of spacecraft damage from dust impacts [*Kelley et al.*, 2014; *Moorhead et al.*, 2014; *Vaubaillon et al.*, 2014; *Tricarico et al.*, 2014]. The effect of dust on Mars was of particular interest for its potential ionospheric effects [*Withers*, 2014], as prior observations of Mars' ionospheric structure identified transient layers attributed to meteor influx [*Withers et al.*, 2008]. Cometary gas impact was also considered for its potential effects on Mars' upper atmosphere [*Yelle et al.*, 2014]. Accurate predictions were challenging due to the lack of precedent: the interval between such near miss events of the observed value of 141,000 km has been estimated at 100,000 years [*Ye and Hui*, 2014]. Dust ejected from the comet was expected to remain confined in a stream that lagged behind the comet in its orbit and was predicted to intercept the planet about 2 h after the comet's closest approach. Dust was expected to impact the hemisphere centered near the morning terminator close to the equator.

The Mars Atmosphere and Volatile EvolutioN (MAVEN) spacecraft entered Mars orbit on 21 September 2014, about a month before the comet encounter, on a mission to study the behavior of the upper atmosphere and the escape of its constituent gases to space [*Jakosky et al.*, 2015]. MAVEN orbits Mars on a 4.5 h elliptical orbit, with a closest approach to Mars' surface at periapse of 150–200 km. Prior to the comet encounter, MAVEN's orbit was phased to place the spacecraft behind Mars (relative to the dust flux) at the predicted time of maximum risk. The spacecraft stopped observations and was commanded into a protective mode. MAVEN restarted observations within 6 h of closest approach, i.e., 4 h after maximum predicted dust passage.

## 2. Observations

MAVEN carries one remote sensing instrument for the study of Mars' upper atmosphere, the Imaging UltraViolet Spectrograph (IUVS) [*McClintock et al.*, 2014]. The instrument captures spectra of the planet and its atmosphere in the far UV (110–190 nm) and mid-UV (190–340 nm), ideal for recording well-known atmospheric emissions from $CO_2$ and its dissociation and ionization products. The instrument is mounted

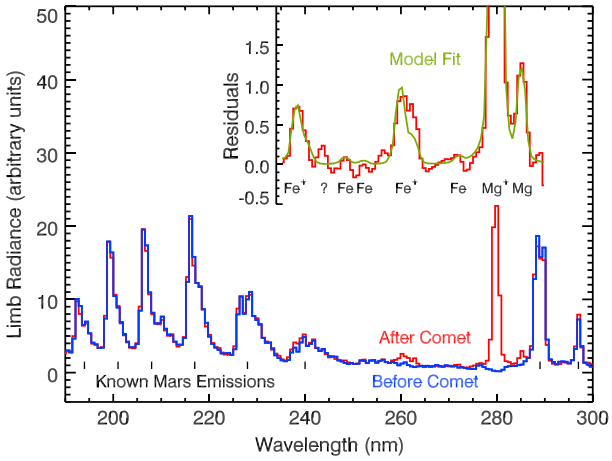


**Figure 1.** Spectra of Mars' atmosphere immediately before and after the closest approach of Comet Siding Spring, taken during Orbit 114 on 19 October 2014 at 15:20:00 UTC and Orbit 116 on 20 October 2014 at 00:35:39 UTC. Both 4.6 s spectra were obtained near a tangent altitude of 119 km at approximately 14 h local time and a solar zenith angle near 60°. Spectra have been scaled and their backgrounds matched. The inset shows a smoothed residual spectrum in red on an expanded vertical scale, obtained by modeling and subtracting known Mars emissions and backgrounds. Numerous emissions from $Mg^+$, Mg, $Fe^+$, and Fe are present, indicated by the overplotted model spectrum. The residual spectrum also suggests that other unidentified features are present. The ±1σ random uncertainty per pixel is ~0.05 in these units.

on an Articulated Payload Platform (APP) that can orient IUVS's field of view relative to Mars depending on spacecraft location, orientation, and desired viewing geometry. During periapse, the APP orients IUVS to look to the side of spacecraft motion, allowing IUVS to use a scan mirror to repeatedly map out the vertical structure of the atmosphere while the spacecraft travels ~90° of arc around the planet. IUVS is capable of other observing modes in other parts of the orbit, but no effects of the comet passage have yet been detected in those data.

IUVS repeated its periapse observations every orbit from MAVEN Orbit 109 (18 October 16:05 UT start time) to Orbit 128 (22 October 07:49 UT), with the exception of Orbit 115 when the spacecraft stood down during maximum predicted dust flux. Data were corrected for detector dark current, scaled according to intensity calibration, and binned in altitude above the surface. Cleaned spectra and vertical profiles of individual emissions were obtained through multiple linear regression fits of independent spectral components, accounting for molecular bands, atomic lines, and reflected solar spectrum background, as well as instrumental resolution and instrumental offsets [*Stevens et al.*, 2011]. Sensitivity calibration is not yet complete, so we bracket the plausible range of emission intensities between the value obtained using preliminary stellar calibrations and that obtained by scaling relative to airglow emissions as measured by the Spectroscopy for Investigation of Characteristics of the Atmosphere of Mars (SPICAM) instrument on Mars Express scaled to the same solar distance and activity [*Leblanc et al.*, 2006]. The factor of two systematic brightness difference between these two calibrations dominates over random errors, so we propagate it as the uncertainty in derived numerical values that follow. But calibration uncertainty has no effect on spectral identifications or relative emission brightnesses associated with geographic, vertical, and temporal variability.

## 3. Results

Figure 1 shows a typical mid-UV spectrum of Mars 3 h prior to Comet Siding Spring's closest approach and 6 h after. Readily apparent in the inset, with the underlying Mars' spectral features subtracted, are new emissions from $Mg^+$, Mg, $Fe^+$, and Fe that were not present before the comet encounter. The brightest emission from the Mars atmosphere for several hours after closest approach was caused by ionized magnesium. Stellar calibration yields a peak intensity of 41 kR for the $Mg^+$ line, while airglow scaling yields a value of 21 kR. While such emissions had never been observed in Mars' atmosphere, the spectrum closely resembles that seen in Earth's upper atmosphere [*Anderson and Barth*, 1971; *Dymond et al.*, 2003] attributed to metal ions and atoms added to the atmosphere through meteor ablation.

All identified metal emissions arise from resonant scattering of solar UV light, rather than direct excitation of the atoms and ions through ablation. $Mg^+$ and $Fe^+$ detection is confirmed by MAVEN's Neutral Gas and Ion Mass Spectrometer (NGIMS) instrument, which detected 10 additional ions [*Benna et al.*, 2015]. The model spectrum was constructed using line positions for the four emitting species, atomic constants for resonant scattering, and the solar MUV spectrum [*Smith et al.*, 1995; *Dymond et al.*, 2003; *Kelleher and Podobedova*, 2008; *McClintock*, 2014; *A'Hearn et al.*, 1983]. In addition to the fainter features identified in Figure 1,

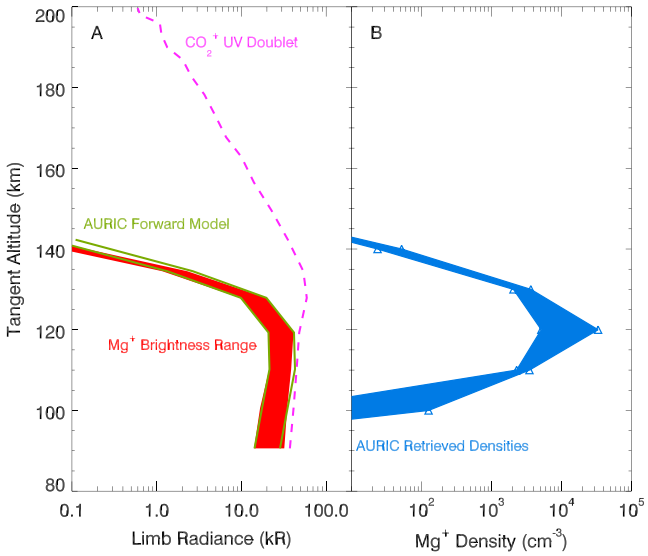


**Figure 2.** (a) Vertical profiles of metal species and $CO_2^+$ obtained from the same scan as Figure 1. The red band shows IUVS $Mg^+$ emission measurements spanning the factor of 2 range of calibration values. The green lines show the best fit to the data using a physical model of the atmosphere and emission physics. The Figure 1 spectrum was obtained at the peak of this scan. (b) Retrieved density profile, with the width of the band indicating the range of retrieved densities consistent with the range of calibration factors. The factor of 2 range in intensity leads to a factor of 6 in ion density due to the nonlinear effects of optically thick radiative transfer. The sharpness of the density peak is exaggerated by the coarse sampling of the retrieval.

several comparably small spectral features persist from spectrum to spectrum but have not yet been identified. In the day preceding the meteor shower, the $Mg^+$ line was undetectable at <4% of its post-comet peak value. No other new features were detected outside this spectral range nor substantial variations in the known Mars' emissions coinciding with the comet passage.

Figure 2a shows a vertical profile of $Mg^+$ emission from one altitude scan of Orbit 116, peaking around 115 km and falling off rapidly with increasing altitude with an exponential scale height of ~2 km. A profile of the $CO_2^+$ UV doublet at 289 nm emission is shown as a fiducial for the background atmosphere and ionosphere, with its peak at 130 km and an ~16 km scale height. Together, these profiles demonstrate that the $Mg^+$ was narrowly confined in a layer 10–20 km below the $CO_2^+$ UV doublet peak located at a few nanobars pressure.

The vertical emission profile can be iteratively modeled to retrieve the underlying density distribution. We used the Atmospheric Ultraviolet Radiance Integrated Code (AURIC) model developed originally for terrestrial use [*Strickland et al.*, 1999] but recently adapted for use at Mars for IUVS retrievals. AURIC uses the REDISTER algorithm [*Gladstone*, 1982] in optically thick cases. The $Mg^+$ emission feature is a doublet, with the stronger line at 279.6 nm twice as optically thick as the weaker line at 280.4 nm. For minimum and maximum calibration values used, we find the optical depth at line center for the stronger line ranges from $\tau = 2.2$ to $\tau = 11$ at 120 km altitude. Figure 2a shows the modeled limb radiance profile, and Figure 2b shows the retrieved density profile. At the calibration minimum and maximum, the peak ionospheric $Mg^+$ density ranges from $5 \times 10^3$ to $3 \times 10^4$ $Mg^+$ ions $cm^{-3}$ around 120 km. We carry this factor of 6 forward as the plausible range of quantities derived from these measurements. The high end of this ion density range is close to the steady state daytime density of the Mars ionosphere but occurs 10–20 km lower than the typical peak altitude.

Figure 3 shows the combination of spatial distribution and temporal evolution of $Mg^+$ emission captured with IUVS observations over one Mars day. Measurements before the comet's passage (Orbit 114, at right) are consistent with little or no $Mg^+$ in the atmosphere. Emission is intense in Orbit 116 and again 4.5 h later on Orbit 117 and generally subsides in Orbit 118 and beyond. The widespread $Mg^+$ distribution evident in Figure 3 indicates a virtually global phenomenon, as opposed to a localized impact region on the planet. In fact, $Mg^+$ is evident in all scans of the first seven orbits (more than one Mars day) after closest approach, suggesting either the dust stream impact lasting at least one Mars rotation or lateral redistribution on the planet on the same time scale. Additional observations, to be described in a later paper, show $Mg^+$ slightly increasing after one Mars rotation and persisting in some regions for up to two Mars days.

Figure 3 (top) shows the vertical distributions from each scan on each orbit. To first order, the profiles are similar with a common peak near 115 km and a scale height of a few kilometers. Deviations from this pattern are evident in later orbits and more northerly latitudes. Nonuniform geographic and vertical

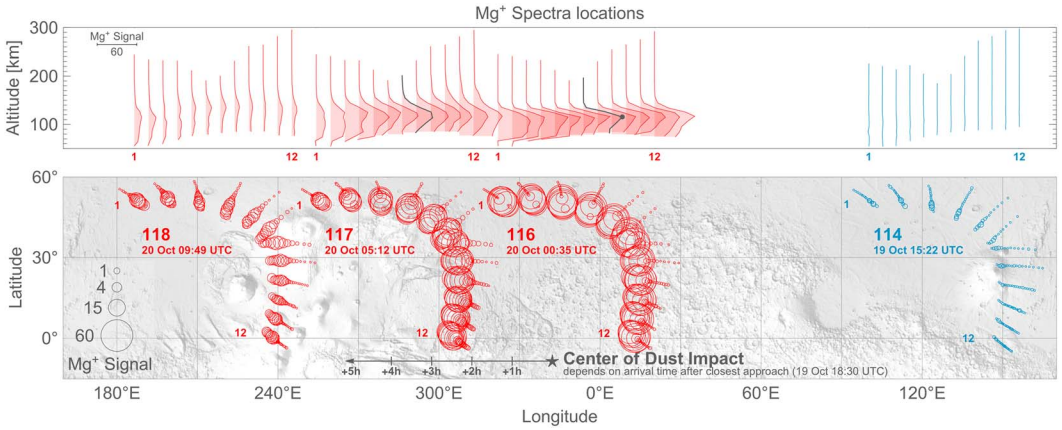


**Figure 3.** (top) Above the map are altitude profiles of the $Mg^+$ emission in relative units. The vertical profiles modeled in Figures 2 and 4 are highlighted with black lines, and the location of the spectrum shown in Figure 1 is indicated with a black dot. (bottom) Spatial distribution and temporal evolution of $Mg^+$ emission. Superposed on a map of Mars are circles whose size represents the relative amount of $Mg^+$ emission present as a function of altitude at different locations on Mars. The circle centers show the locations below the line of sight tangent points during the altitude scan. Each swath across the planet is composed of 12 altitude scans made during a single periapse pass, starting at the time indicated at northern latitudes and passing south to the equator over 22 min. The first observations are shown at right, with successive swaths appearing to the left (west) as the rotation of the planet carries those regions into the IUVS field of view. The series starts at right with Orbit 114, followed by an observing gap during Orbit 115, then the detection of bright emissions in Orbit 116 and subsequent decline. The star at bottom indicates the direction of the relative velocity between Mars and the comet at the moment of closest approach and the motion of this point in the following hours.

distributions could be caused either by uneven deposition of dust on the atmosphere, winds and other transport processes, variable rates of chemical reactions which remove $Mg^+$, or some combination.

## 4. Conclusions

Observations of meteoric ions in Mars' atmosphere can offer profound insights into the nature of comets and of Mars' atmosphere. Numerical modeling of the ablation process can match the initial vertical profile of $Mg^+$, as shown in Figure 4. We use CABMOD (Chemical Ablation Model) [*Vondrak et al.*, 2008] validated in terrestrial studies, which includes heating and melting of dust particles from collisions with the ambient atmosphere, evaporation of atoms from the molten particle surface, and prompt ionization caused by collisions with the ambient gas at the dust relative velocity of 56 km/s. The vertical profiles of the injected metals are input into a 1-D atmospheric model [*Whalley and Plane*, 2010], which contains detailed chemistry of magnesium and iron based on laboratory studies of pertinent reaction rates including photoionization and charge exchange. The model contains turbulent (eddy) diffusion up to the Mars turbopause (~135 km) and the ambipolar diffusion of metal ions above. While the matches to both vertical profiles are good,

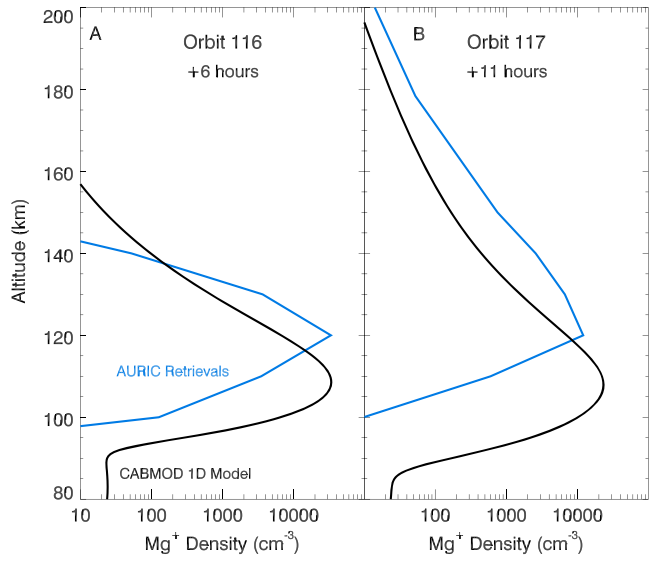


**Figure 4.** Retrieved $Mg^+$ density profiles from AURIC compared to CABMOD/1-D model output profiles. The left model profile more closely resembles the initial injection of $Mg^+$ into the atmosphere, and the right profile shows its subsequent evolution in the atmosphere.

the CABMOD model generally predicts lower-altitude deposition by 5–10 km. The observed and modeled transport of $Mg^+$ to higher altitudes on Orbit 117 is good agreement with an in situ mass spectrometric measurement by the Neutral Gas and Ion Mass Spectrometer instrument on MAVEN on subsequent orbits [*Benna et al.*, 2015].

The ionospheric density profiles retrieved by AURIC (Figure 2, using the higher end values) and modeled by CABMOD/1-D model (Figure 4a) are comparable to the profiles reported by the Mars Advanced Radar for Subsurface and Ionosphere Sounding (MARSIS) instrument on Mars Express [*Gurnett et al.*, 2015] and Shallow Radar on Mars Reconnaissance Orbiter [*Restano et al.*, 2015], both attributed to the Comet Siding Spring meteor shower. There are some significant differences which merit further analysis. In particular, the MARSIS-observed ionospheric layer appears to lie at lower altitudes than the metal ion layer we report. It remains to be seen whether this difference means that two distinct layers are present, whether the ionospheric layer is different at the times and places observed, or whether the two independent methods of detection are biased to yield somewhat different results. Similarly, the profiles derived here are comparable in density but higher in altitude to ionospheric profiles attributed to meteor ablation on Mars in the past [*Withers et al.*, 2008] and predicted for Comet Siding Spring [*Withers*, 2014].

Our atmospheric model follows the chemical evolution of meteoric metals and their reaction with background gases. In the model, $Mg^+$ recombines by forming clusters with $CO_2$ that then undergo dissociative recombination with electrons [*Whalley and Plane*, 2010]. One important consequence of this recombination pathway is that the modeled column abundance of Mg between 100 and 120 km reaches ~50% that of $Mg^+$ after about 12 h. Since the UV scattering efficiency of Mg is about 3 times larger than that of $Mg^+$, the model predicts that as time progresses, Mg emission should exceed that from $Mg^+$. This is not observed, and the continuous low brightness of Mg emission suggests that either $Mg^+$ is being destroyed without creating Mg or that Mg itself is lost as rapidly as it forms. Either way, the observations provide strong evidence that chemical pathways at Mars are significantly different than at Earth. The eventual fate of the metals deposited in Mars' atmosphere by Comet Siding Spring will be to form neutral compounds (oxides, hydroxides, and carbonates) that then polymerize into particles known as meteoric smoke [*Saunders and Plane*, 2006]. These aerosols may persist in the Mars atmosphere for years, as they do at Earth [*Dhomse et al.*, 2013], interacting with sunlight with potentially significant effects.

Another Earth-Mars difference bears closer examination. On Earth, the continuous arrival of sporadic meteors (those not associated with any meteor shower) creates an omnipresent metal layer in Earth's atmosphere [*Langowski et al.*, 2015]. This layer is sufficiently dense that the addition of metallic material in meteor showers is small by comparison and is challenging to detect by in situ measurements [*Grebowsky et al.*, 1998] and never detected by remote sensing. By contrast, a steady state layer from sporadics has never been detected at Mars, while Comet Siding Spring created a readily observable phenomenon. This apparent discrepancy could be explained by (1) the extreme nature of the Siding Spring event, (2) an intrinsically small supply of sporadic meteors at Mars, or (3) unidentified metal loss processes preventing the accumulation of detectable amounts from sporadics. Deeper searches are underway for steady state emission below the IUVS 4% upper limit and for other meteor shower events; these could distinguish among the possibilities above.

The critical sensitivities in the CABMOD model are the particle size, density, and the total dust deposition. Submicron-sized particles are slowed high in the atmosphere and never heat enough to ablate. Conversely, particles larger than 100 μm penetrate to altitudes below 105 km before significant ablation occurs. In order to produce a layer of $Mg^+$ between 105 and 120 km, the cometary dust particles need to be small (radius $< 100$ μm) and low density ($<1$ g cm$^{-3}$, characteristic of fractal-like agglomerates). These properties are consistent with the bottom end of the range of cometary dust particles collected in Earth's stratosphere [*Brownlee*, 1978]. Particles of this size, however, were expected to miss Mars based on their estimated ejection velocities and the influence of radiation pressure [*Kelley et al.*, 2014; *Moorhead et al.*, 2014; *Tricarico et al.*, 2014]. This may indicate that small dust particles were ejected at velocities above 3 m s$^{-1}$.

The 1-D model match to the Orbit 116 profile requires a dust deposition of $0.4–2.2 \times 10^{-7}$ g/m$^2$, depending on the calibration used and assuming a cosmic dust composition of 10.3% magnesium by mass. Applied hemispherically, the total mass deposited on Mars would have been 2700–16,000 kg. We can place the magnitude of the Siding Spring event in context by comparing our derived mass with predictions and with terrestrial meteor showers. While our observations do not directly constrain the population of particles

>1 mm which create easily visible shooting stars, we can roughly estimate their abundance assuming a dust size distribution function with a power law exponent of −2.6 [*Moorhead et al.*, 2014]. We find that the deposition fluence at Mars of particles larger than 1 mm is $0.5–3\times10^{-6}\,m^{-2}$. The top of our range is 30 times larger than some predictions [*Tricarico et al.*, 2014] but factors of 1200 and 24,000 times smaller than others [*Moorhead et al.*, 2014; *Vaubaillon et al.*, 2014]. A human observer under good conditions (area of sky seen by naked eye $=3.7\times10^{4}\,km^{2}$) would therefore have observed a zenith hourly rate of ~$0.2–1\times10^{5}$ visible meteors per hour (or 5–30 meteors per second) for more than an hour. Such an intense meteor shower has not been observed globally in modern times on Earth, although the Leonid meteor shower of 1833 may have been comparable [*Asher*, 1999]. The intensity of the Comet Siding Spring meteor shower, coupled with Mars' lack of a significant steady state metal layer, makes this event a unique window into understanding major perturbations to a planetary atmosphere.

**Acknowledgments**

The MAVEN mission is supported by NASA in association with the University of Colorado and NASA's Goddard Space Flight Center. We gratefully acknowledge the mission control team at Lockheed Martin who returned MAVEN to normal operations as rapidly as possible after the comet's passage, making these irreplaceable observations possible. IUVS appreciates the efforts of its operations team for their rapid preparation of observing sequences and subsequent data processing and analysis. The authors thank Michael Kelley for the useful discussion on cometary dust. A.S. is supported by the Belgian American Educational Foundation and the Rotary District 1630. J.M.C.P. and J.D.C.S. are supported by the European Research Council (project 291332-CODITA). M.H.S. is supported by the NASA MAVEN Participating Scientist program. The data will be publicly archived at the Planetary Atmospheres node of the Planetary Data System.

The Editor thanks Jean-Claude Gérard and an anonymous reviewer for their assistance in evaluating this paper.

## References

A'Hearn, M. F., J. T. Ohlmacher, and D. G. Schleicher (1983), A high resolution solar atlas for fluorescence calculations, *Tech. Rep. AP83-044*, Univ. of Maryland.

Anderson, J. G., and C. A. Barth (1971), Rocket investigation of the Mg I and Mg II dayglow, *J. Geophys. Res.*, *76*, 3723–3732, doi:10.1029/JA076i016p03723.

Asher, D. J. (1999), The Leonid meteor storms of 1833 and 1966, *Mon. Not. R. Astron. Soc.*, *307*, 919–924.

Benna, M., P. R. Mahaffy, J. M. Grebowsky, J. M. C. Plane, R. V. Yelle, and B. M. Jakosky (2015), Metallic ions in the upper atmosphere of Mars from the passage of Comet Siding Spring, *Geophys. Res. Lett.*, *42*, doi:10.1002/2015GL064120.

Brownlee, D. E. (1978), Interplanetary dust: Possible implications for comets and presolar interstellar grains, in *Protostars and Planets*, edited by T. Gehrels, pp. 134–150, Univ. of Ariz. Press, Tucson.

Dhomse, S. S., R. W. Saunders, W. Tian, M. P. Chipperfield, and J. M. C. Plane (2013), Plutonium-238 observations as a test of modeled transport and surface deposition of meteoric smoke particles, *Geophys. Res. Lett.*, *40*, 4454–4458, doi:10.1002/grl.50840.

Dymond, K. F., K. D. Wolfram, S. A. Budzien, A. C. Nicholas, R. P. McCoy, and R. J. Thomas (2003), Middle ultraviolet emission from ionized iron, *J. Geophys. Res.*, *30*(1), 1003, doi:10.1029/2002GL015060.

Gladstone, G. R. (1982), Radiative transfer with partial frequency redistribution in inhomogeneous atmospheres: Application to the Jovian aurora, *JQSRT*, *27*, 545–556.

Grebowsky, J. M., R. A. Goldberg, and W. D. Pesnell (1998), Do meteor showers perturb the ionosphere, *J. Atmos. Space Phys.*, *60*, 607–615.

Gurnett, D. A., D. D. Morgan, A. M. Persoon, L. J. Granroth, A. J. Kopf, J. J. Plaut, and J. L. Green (2015), An ionized layer in the upper atmosphere of Mars caused by dust impacts from Comet Siding Spring, *Geophys. Res. Lett.*, *42*, doi:10.1002/2015GL063726.

Jakosky, B., et al. (2015), The 2013 Mars Atmosphere and Volatile Evolution (MAVEN) mission to Mars, *Space Sci. Rev.*, doi:10.1007/s11214-015-0139-x.

Kelleher, D. E., and L. I. Podobedova (2008), Atomic transition probabilities of sodium and magnesium: A critical compilation, *J. Phys. Chem. Ref. Data*, *37*, 267–706.

Kelley, M. S. P., T. L. Farnham, D. Bodewits, P. Tricarico, and D. Farnocchia (2014), A study of dust and gas at Mars from comet C/2013 A1 (Siding Spring), *Astrophys. J. Lett.*, *792*, L16, doi:10.1088/2041-8205/792/1/L16.

Langowski, M. P., C. von Savigny, J. P. Burrows, W. Feng, J. M. C. Plane, D. R. Marsh, D. Janches, M. Sinnhuber, A. C. Aikin, and P. Liebing (2015), Global investigation of the Mg atom and ion layers using SCIAMACHY/Envisat observations between 70 and 150 km altitude and WACCM-Mg model results, *Atmos. Chem. Phys.*, *15*, 273–295.

Leblanc, F., J. Y. Chaufray, J. Lilensten, O. Witasse, and J.-L. Bertaux (2006), Martian dayglow as seen by the SPICAM UV spectrograph on Mars Express, *J. Geophys. Res.*, *111*, E09S11, doi:10.1029/2005JE002664.

McClintock, B. (2014), SORCE SOLSTICE FUV level 3 solar spectral irradiance daily means, version 013, NASA Goddard Earth Sci. Data and Inf. Services Cent. (GES DISC), Greenbelt, Md. [Available at http://disc.sci.gsfc.nasa.gov/datacollection/SOR3SOLFUVD_V013.html.]

McClintock, W. E., N. M. Schneider, G. M. Holsclaw, A. C. Hoskins, I. Stewart, J. Deighan, J. T. Clarke, F. Montmessin, and R. V. Yelle (2014), The Imaging Ultraviolet Spectrograph (IUVS) for the MAVEN mission, *Space Sci. Rev.*, doi:10.1007/s11214-014-0098-7.

Moorhead, A. V., P. A. Wiegert, and W. J. Cooke (2014), The meteoroid fluence at Mars due to comet C/2013 A1 (Siding Spring), *Icarus*, *231*, 13.

Restano, M., J. J. Plaut, B. A. Campbell, Y. Gim, D. Nunes, F. Bernardini, A. Egan, R. Seu, and R. J. Phillips (2015), Effects of the passage of comet C/2013 A1 (Siding Spring) observed by the Shallow Radar (SHARAD) on Mars Reconnaissance Orbiter, *Geophys. Res. Lett.*, *42*, doi:10.1002/2015GL064150.

Saunders, R. W., and J. M. C. Plane (2006), A laboratory study of meteor smoke analogues: Composition, optical properties and growth kinetics, *J. Atmos. Sol. Terr. Phys.*, *68*, 2182–2202.

Smith, P. L., C. Heise, J. R. Esmond, and R. L. Kurucz (1995), Atomic spectral line database [from CD-ROM 23 of R.L. Kurucz], Smithsonian Astrophysical Observatory, Cambridge. [Available at http://cfa-www.harvard.edu/amp.]

Stevens, M. H., et al. (2011), The production of Titan's ultraviolet nitrogen airglow, *J. Geophys. Res.*, *116*, A05304, doi:10.1029/2010JA016284.

Strickland, D. J., J. Bishop, J. S. Evans, T. Majeed, P. M. Shen, R. J. Cox, R. Link, and R. E. Huffman (1999), Atmospheric Ultraviolet Radiance Integrated Code (AURIC): Theory, software architecture, inputs, and selected results, *JQSRT*, *62*, 689–742.

Tricarico, P., N. H. Samarasinha, M. V. Sykes, J.-Y. Li, T. L. Farnham, M. S. P. Kelley, D. Farnocchia, R. Stevenson, J. M. Bauer, and R. E. Lock (2014), Delivery of dust grains from comet C/2013 A1 (Siding Spring) to Mars, *Astrophys. J. Lett.*, *787*, L35, doi:10.1088/2041-8205/787/2/L35.

Vaubaillon, J., L. Maquet, and R. Soja (2014), Meteor hurricane at Mars on 2014 October 19 from comet C/2013 A1, *Mon. Not. R. Astron. Soc.*, *439*, 3294–3299.

Vondrak, T., J. M. C. Plane, S. L. Broadley, and D. Janches (2008), A chemical model of meteoric ablation, *Atmos. Chem. Phys.*, *8*, 7015–7031.

Whalley, C. L., and J. M. C. Plane (2010), Meteoric ion layers in the Martian atmosphere, *Faraday Discuss.*, *147*, 349–368.

Withers, P. (2014), Predictions of the effects of Mars's encounter with comet C/2013 A1 (Siding Spring) upon metal species in its ionosphere, *Geophys. Res. Lett.*, *41*, 6635–6643, doi:10.1002/2014GL061481.

Withers, P., M. Mendillo, D. P. Hinson, and K. Cahoy (2008), Physical characteristics and occurrence rates of meteoric plasma layers detected in the Martian ionosphere by the Mars Global Surveyor Radio Science Experiment, *J. Geophys. Res.*, *113*, A12314, doi:10.1029/2008JA013636.

Ye, Q.-Z., and M.-T. Hui (2014), An early look of comet C/2013 A1 (Siding Spring): Breathtaker or nightmare?, *Astrophys. J.*, *787*, 115.

Yelle, R., A. Mahieux, S. Morrison, V. Vuitton, and S. M. Hörst (2014), Perturbation of the Mars atmosphere by the near-collision with comet C/2013 A1 (Siding Spring), *Icarus*, *237*, 202–210, doi:10.1016/j.icarus.2014.03.030.